Article

Prosthetist-Specific Rectification Templates Based on Artificial Intelligence for the Digital Fabrication of Custom Transtibial Sockets

Andrea Giovanni Cutti, Maria Grazia Santi, Andrew H. Hansen, Stefania Fatone and Residual Limb Shape Capture Group

Article

Prosthetist-Specific Rectification Templates Based on Artificial Intelligence for the Digital Fabrication of Custom Transtibial Sockets

Andrea Giovanni Cutti [1], Maria Grazia Santi [2], Andrew H. Hansen [3,4], Stefania Fatone [5,6,*]
and Residual Limb Shape Capture Group [†]

1 INAIL, 40054 Vigorso di Budrio, BO, Italy; ag.cutti@inail.it
2 Department of Industrial Engineering, University of Padova, 35131 Padova, PD, Italy;
  mariagrazia.santi@phd.unipd.it
3 Minneapolis VA Health Care System, Minneapolis, MN 55417, USA; andrew.hansen2@va.gov
4 Department of Family Medicine and Community Health, Department of Biomedical Engineering,
  University of Minnesota, Minneapolis, MN 55455, USA
5 Northwestern University Prosthetics Orthotics Center, Department of Physical Medicine and Rehabilitation,
  Northwestern University, Chicago, IL 60611, USA
6 Department of Rehabilitation Medicine, University of Washington, Seattle, WA 98195, USA
* Correspondence: sfaton@uw.edu; Tel.: +1-206-685-7918
† Membership of the Residual Limb Shape Capture Group is provided in the Acknowledgments.

Abstract: The socket is the most important, patient-specific element of a prosthesis. Conventionally, the process of making a custom socket involves manually rectifying a plaster model of the residual limb. This process is time-consuming and often inconsistent among prosthetists because it is based on implicit knowledge. Hence, the aim of this work was to describe a novel process of generating a prosthetist-specific, digital "global" template and to illustrate that it can be automatically applied to rectify the shape of a transtibial residual limb. The process involved (1) the acquisition of a "training" dataset of unrectified and rectified positive models through manual data collection and digital 3D scanning, and (2) the unsupervised learning of the prosthetist's rectifications by an artificial intelligence (AI) algorithm. The assessment of the process involved (1) evaluating whether the rectification rule learned by the AI was consistent with the prosthetist's expectations, and (2) evaluating the template feasibility by applying the AI rectification process to a new residual limb and comparing the results to the prosthetist's manual rectification for the same residual limb. The results suggest that the AI-rectified positive was consistent with the approach described by the prosthetist, with only small radial and angle errors and similar dimensions (volume and cross-sectional perimeters) as the hand-rectified positive. This study provides a proof-of-concept of the ability to integrate an AI algorithm into the fabrication process for transtibial prosthetic sockets. Once refined, this approach may provide a time-saving tool for prosthetists by automatically implementing typical rectifications and providing a good starting socket fit for individuals with amputation.

Keywords: prosthetic socket; amputation; artificial intelligence; digital rectification; transtibial; CAD-CAM

1. Introduction

The socket is the most important, patient-specific element of a lower-limb prosthesis because it is the customized interface between the residual limb of a person with amputation and the mass-produced prosthetic components, e.g., the foot, joints, and interconnecting modules [1–3]. Prosthetists begin socket construction with the "casting phase", aiming to obtain an "impression" or "negative model" of the residual limb. This negative model is later transformed into a positive "raw" model (often made of plaster), also referred to as the "unrectified positive" (UP). Prosthetists then shape the UP by either adding or removing

material depending on the specific anatomical region. This process is typically referred to as "rectification" and the resultant model is referred to as the "rectified positive" (RP) [4–9]. The socket is then fabricated using the RP, either by vacuum-forming a thermoplastic, composite material lamination or by 3D printing, and then assessed on the patient while standing and walking. During this last phase, the socket volume and shape are fine-tuned, typically through a set of limited changes, to ensure the socket is comfortable. A well-fitting socket preserves the integrity and health of soft tissues and allows for the reliable and effective control of the prosthesis during daily life activities [2,3].

Over the years, prosthetists have developed different casting and rectification techniques to reach these clinical goals reliably and efficiently, adjusting to improved knowledge of socket design, innovations in socket materials and interface components (e.g., liners and suspension systems), and socket fabrication technologies [2,7,10–16]. Unfortunately, the overall process is often inconsistent among prosthetists because it is based on implicit knowledge determined by personal experience, skills, and opinions [4,6]. Also, it is difficult to quantify and communicate the rectifications implemented on any single positive model, hindering the sharing of techniques between prosthetists [6].

Since the 1980s, prosthesis manufacturing has moved toward the digitization of processes [9,17]. Firstly, scanning techniques were introduced to acquire the socket/lower-limb/positive model shapes in mesh format, and then computer-aided design (CAD) software was adopted to perform rectifications digitally [18–26]. The ability to store, view, and modify meshes in a virtual environment brought benefits, including (1) the repeatability and documentation of production steps, (2) reduced physical storage space, (3) reduced fabrication time [9,27], (4) reduced exposure of prosthetists to irritant physical agents (e.g., water [28] and plaster [29]) and biomechanical factors (e.g., lifting heavy objects and changing postures) [30], (5) the introduction of templates to record and repeat an ordered set of CAD operations [6], and (6) the ability to communicate (teach) rectification approaches [7]. For this last benefit, "rectification color maps" (RCMs) consisting of a 3D mesh of a residual limb are typically generated to visually describe different rectification methods [31–36]. Visual inspection of RCMs has demonstrated utility as a teaching aid [7,31,37,38], for comparing rectification methods, and when implementing new templates for computer-aided design–computer-aided manufacturing (CAD-CAM) [7,31]. However, RCMs are usually reported for a pre-identified representative person with amputation rather than representing a well-defined, statistical mean rectification over a pool of subjects.

Despite this limitation, the availability of templates for different socket designs has allowed prosthetists to semi-automatically perform, in a digital environment, the typical rectifications performed on a UP to obtain the respective RP. However, templates (macro- or customized libraries) as available in commercial software such as Canfit (Vorum, Vancouver, BC, Canada), BioShape (BioSculptor, Hialeah, FL, USA), Fitflow (Rodin4D, Nouvelle-Aquitaine, France), ORTEN (Proteor, Dijon, France), or OMEGA (WillowWood, Mt. Sterling, OH, USA), rely on operator input to adapt the template to the specific patient's residual limb dimensions. In particular, they require prosthetists to manually identify the location of the desired rectification over each anatomical region and to scale the extent of the rectification in each region. Moreover, each "region" is independent from the other, and their relationships remain unknown. Furthermore, current templates are based on explicit knowledge and do not capture the implicit rectification strategies that specific prosthetists apply. Overall, it is not currently possible using commercially available software to apply templates to perform rectifications automatically and globally over the entire residual limb of a new patient. Overcoming these limitations may reduce the rectification time and make it possible to apply the templates of highly skilled prosthetists in resource-limited areas without sufficiently skilled prosthetists. The time saved on newly automated processes may be spent by the prosthetist interacting with the patient to better understand their needs and improving the socket shape and volume during static and dynamic fitting.

This work aims to address these gaps by describing an original experimental and digital process to generate and use prosthetist-specific "global" templates to predict the

shape of a first-attempt patient-specific socket. To illustrate the potential of this approach, an example application is reported using a dataset of information extracted from the manufacturing process of fifteen total surface-bearing sockets for subjects with transtibial amputation taken from a larger clinical trial [39].

2. Materials and Methods

2.1. Digital Process to Generate a Prosthetist-Specific "Global" Template

The process to generate a prosthetist-specific "global" template involved (1) the acquisition of a "training" dataset of UPs and RPs through (a) manual data collection and (b) digital 3D scanning, and (2) the unsupervised learning of the rectifications by an artificial intelligence (AI) algorithm.

(1a) Manual data collection of training dataset

The first phase of the process consisted of manually fabricating UPs and RPs for a pool of individuals with amputation. Since the objective of this study was to build a prosthetist-specific "global" template, the same prosthetist performed the casting and rectification procedures for all individuals.

The manual procedure started with the identification of landmarks (LMs) on the participant's liner–clad residual limb using LMs identified by the consensus of all prosthetists involved in the larger clinical trial [39]. The LMs were based on those typically identified by prosthetists during the routine hand-casting of residual limbs (Figure 1). The identification of LMs (step 1, Figure 2) was crucial for creating reference points for the later spatial registration of the scans and for tracking shape changes. Next, a transparent film (e.g., cling wrap) was wrapped over the liner and the LMs were marked on the film with a felt-tip pen (step 2, Figure 2). Wet plaster bandages were then wrapped around the participant's residual limb and, while the plaster was curing, the prosthetist manually applied pressure to obtain a "negative" model with the initial shape of the intended socket design (step 3, Figure 2). During casting, the ink markings of the LMs were transferred from the film to the inside of the negative model.
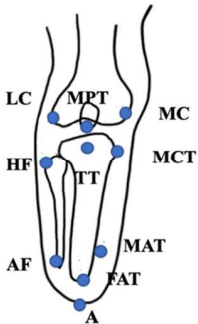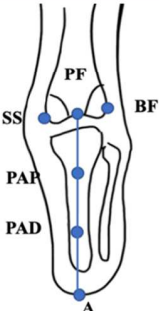

LANDMARK POSITIONING	ABBREVIATION	DEFINITION
Anterior view	MPT	Mid Patellar Tendon
	LC	Lateral Condyle (of the femur)
	MC	Medial Condyle (of the femur)
	TT	Tibial Tuberosity
	HF	Head of the Fibula
	MCT	Medial Condyle of the Tibia
	FAT	Anterior distal end of Tibia
	AF	Distal end of Fibula
	MAT	Medial distal end of Tibia
Posterior view	PF	Popliteal Fossa
	SS	Below the semitendinosus/semimembranosus at knee flexed 90°
	BF	Below the biceps femoris at knee flexed 90°
	PAP	1/3 of the P-A distance - proximal
	PAD	1/3 of the P-A distance - distal
	A	Most distal end of the residual limb

Figure 1. Landmarks identified and marked by the prosthetist on participants' liner–clad residual limbs.

Figure 2. Schematic representation of the manual data collection required to create the training dataset (steps 1–7) and the final diagnostic socket fabricated to allow for the evaluation of the process (step 8). LMs: landmarks; UP: unrectified positive; RP: rectified positive.

Once the negative model was removed from the participant's residual limb, a 15 cm extension made of plaster bandages was added proximally (step 4, Figure 2). To transfer the LMs between the negative and positive model, polyurethane circular markers (2 mm thick with a 6 mm diameter) were glued with a hot glue gun to the inner surface of the negative model corresponding to the ink markings (step 5, Figure 2). To later ensure the spatial registration of the scans, an additional twenty polyurethane markers were randomly placed and glued to the inner surface of the proximal extension. The negative model was then filled with liquid plaster to obtain the UP (step 6, Figure 2). Once the liquid plaster hardened, the plaster bandages were removed, resulting in a UP with indentations corresponding to the LMs originally identified on the participant's residual limb.

At the study commencement, the prosthetist provided a written description of their rectification approach for what they described as a total surface-bearing socket (reported in words and graphical illustration in Figure 3). The prosthetist rectified the UP, removing and adding plaster from specific anatomical regions in accordance with the intended socket design, but leaving untouched the proximal extension (step 7, Figure 1).

(1b) Digital 3D scanning of training dataset

The next phase of the process consisted of digitally scanning the UP and RP pairs obtained during the manual data collection. In this study, the EinScan Pro 2X Plus structured light scanner coupled with the high-definition accessory was used (Shining3D, Hangzhou, China). This scanner is reported by the manufacturer to have a volumetric accuracy in the VDI/VDE 2634 Standards [40] of less than 0.05 mm. Additionally, this scanner was previously reported to be accurate, repeatable, and reproducible for quantitative shape analysis in the evaluations of residual limb models [41]. During scanning, each plaster model (UP or RP) was placed on a rotating turntable and the scanner was held stationary by an operator while pointing at the surface of the rotating model. Each UP-RP pair was linked by virtue of having LMs in the proximal extension that remained unchanged during

the rectification process. This was fundamentally important for the spatial registration of the meshes, as they represent common reference points on separate scans.
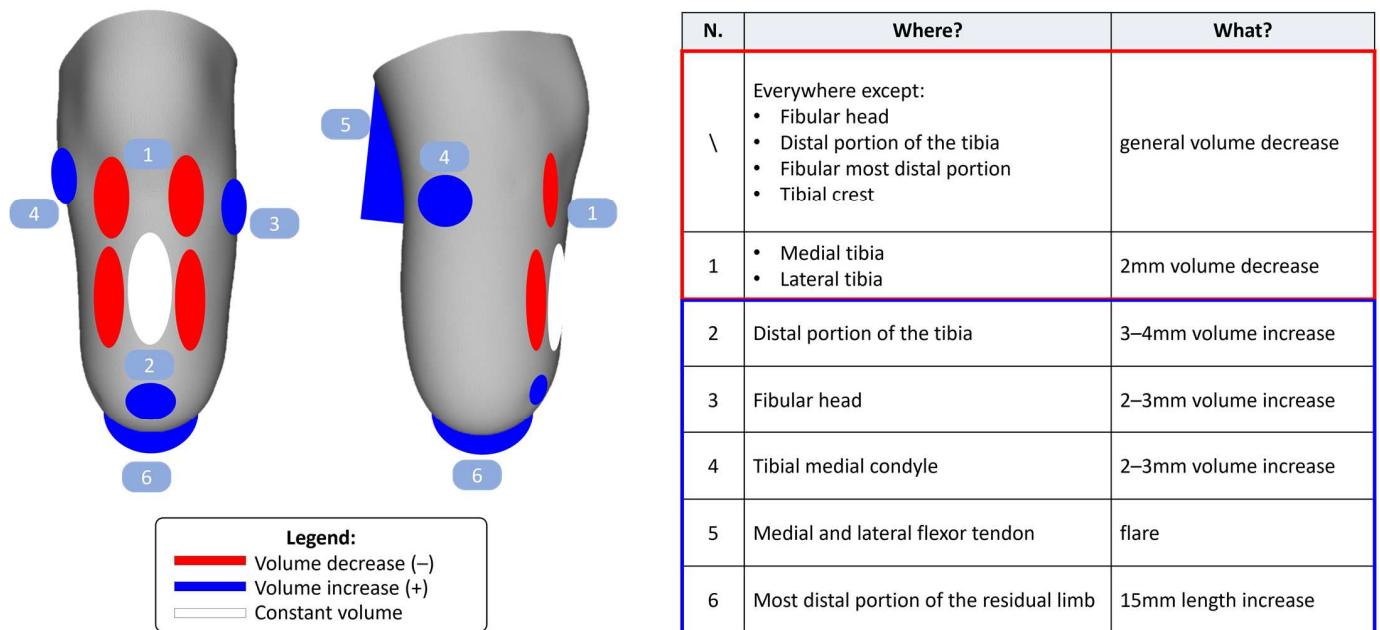

N.	Where?	What?
\	Everywhere except: • Fibular head • Distal portion of the tibia • Fibular most distal portion • Tibial crest	general volume decrease
1	• Medial tibia • Lateral tibia	2mm volume decrease
2	Distal portion of the tibia	3–4mm volume increase
3	Fibular head	2–3mm volume increase
4	Tibial medial condyle	2–3mm volume increase
5	Medial and lateral flexor tendon	flare
6	Most distal portion of the residual limb	15mm length increase

Legend:
Volume decrease (−)
Volume increase (+)
Constant volume

Figure 3. Prosthetist-specific rectification template. Red shading is associated with a volume decrease, blue shading is associated with a volume increase, and white shading represents unmodified areas (constant volume). The embedded table summarizes the prosthetist's description of their rectification approach.

2.2. Unsupervised Learning of the Rectifications by an Artificial Intelligence (AI) Algorithm

The UP-RP pairs of the meshes for each participant were then digitally processed to build a "global template". Digital processing was performed using custom Python software (version 3.8) that takes advantage of MeshLab [42] (MeshLab_64bit_fp v2020.07) and VTK libraries [43] (version 9.0.0) as computational geometry engines, with Qt [44] (PyQt5 version 5.14.2) to support the graphical user interface [41].

Template calculation involved the ten steps illustrated in Figure 4. First, it was necessary to identify and label the location of each LM on the UP-RP mesh pairs (step 1, Figure 4). For each LM, labeling required associating the marker label with the relative vertex identifier (ID) of the mesh. The proximal extension labels were arbitrarily established, and the same labels were used for the corresponding proximal extension landmarks on the UP-RP mesh pairs.

Next, the UP meshes were aligned in the global coordinate system using LMs (e.g., the mid-patellar tendon (MPT), the popliteal fossa (PF), the distal end of the residual limb (A), and the anterior distal end of the tibia (FAT)) that correspond to certain axes and planes (step 2, Figure 4) using an alignment procedure reported in Appendix A.

Next, the RPs were spatially registered to their respective UPs (step 3, Figure 4). First, a rigid approach was used based on Singular Value Decomposition (SVD) [45] using homologous markers (i.e., markers related to the same geometrical point, identified on the UP and transferred on the RP). Then, to further improve the registration, the iterative closest point (ICP) algorithm [46] was applied only to the proximal extension vertices given that they were identical on the UP-RP pairs [41].

Next, the proximal extensions of both the UP and RP meshes were removed with 3D mesh editing software (Geomagic version 1.0.0.34, Morrisville, NC, USA) (step 4, Figure 4) and the indentations in the UP scans, created by the glued physical markers, were closed. Both the UP and RP meshes were smoothed to avoid any duplicated and unreferenced faces or vertices (step 5, Figure 4). Since smoothing changed the mesh topology, and consequently the vertex IDs, it was necessary to project the LMs from the pre-smoothed

mesh to the post-smoothed mesh and to associate the LM labels to the new vertex IDs (step 6, Figure 4). Next, it was necessary to ensure that all of the meshes had the same laterality. Consequently, all of the right-limb UPs and RPs were mirrored to obtain a dataset comprising of only left-limb meshes (step 7, Figure 4).
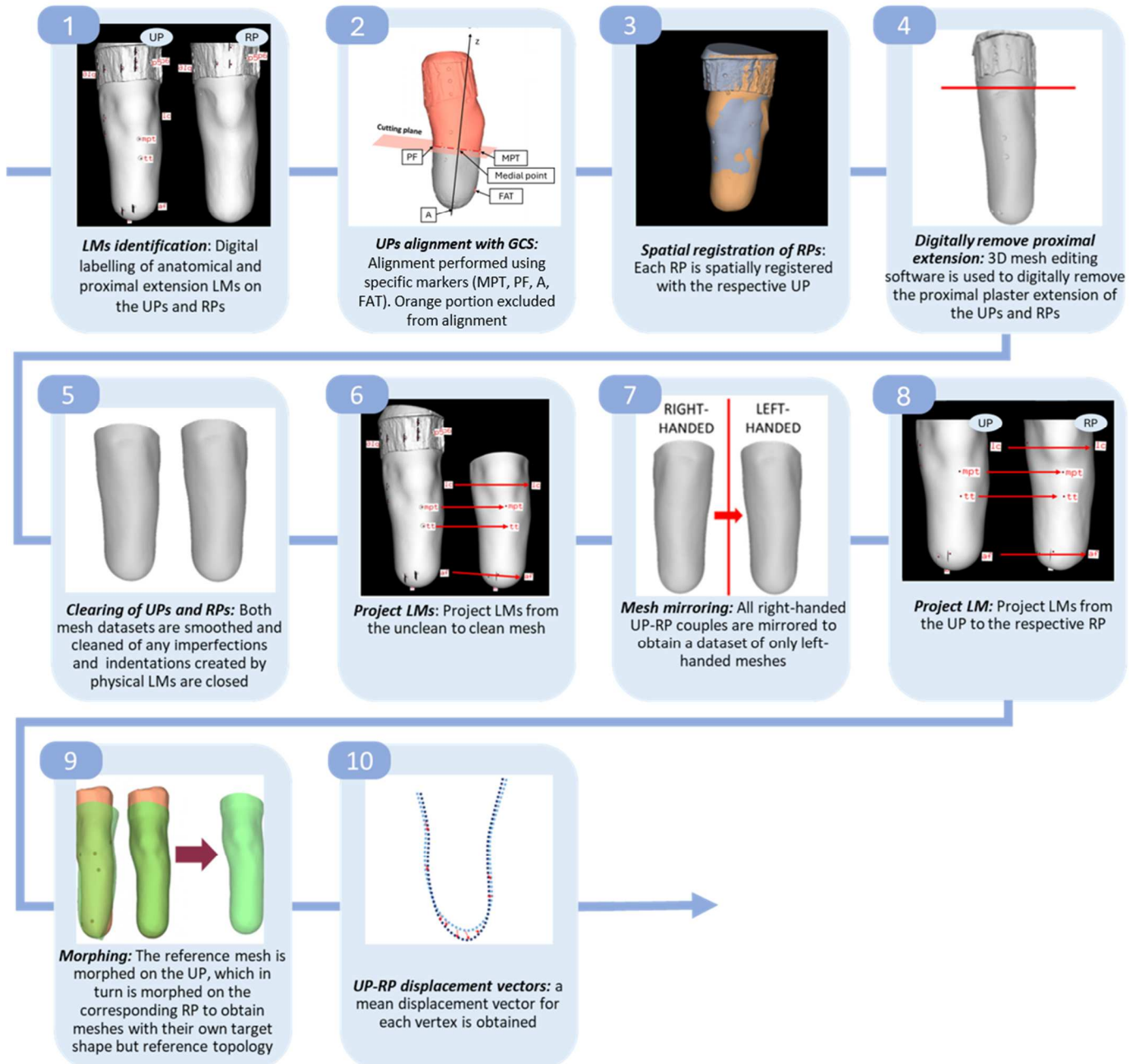

Figure 4. Schematic representation of template calculations to produce a prosthetist-specific rectification template. LMs: landmarks; UP: unrectified positive; RP: rectified positive; GCS: global coordinate system; MPT: mid-patella tendon; PF: popliteal fossa; A: distal end of the residual limb; FAT: anterior distal end of the tibia; 3D: three-dimensional.

Then, the LMs labeled in step 1 were projected from each UP to the respective RP to digitally identify the anatomical LMs that were no longer physically visible on the RP after the rectification process (step 8, Figure 4).

Next, a pre-defined "Reference Mesh", characterized by a homogeneous topology, was "morphed" onto the UP meshes and each of these morphed meshes were in turn morphed onto the corresponding RP mesh (step 9, Figure 4) using the Radial Basis Function method

(RBF-Morph, Rome, Italy). The outputs of this procedure were two meshes characterized by the same topology (vertices and faces), the Reference Mesh, and the shape of the "target" meshes, i.e., the UP and RP, respectively [47]. Further technical details about the creation of the Reference Mesh and morphing step are reported in Appendix A.

Finally, for each UP-RP pair, displacement vectors between homologous vertices were assessed (step 10, Figure 4). An unsupervised artificial intelligence (AI) algorithm, specifically Principal Component Analysis (PCA), was applied to all of these vectors using the approach described by Dickinson et al. [34]. This algorithm was able to extract the average displacement, referred to in the following as the average displacement matrix (ADM), and to learn and cluster the "modes of variation", i.e., the synergistic changes the prosthetist applies when adapting their typical rectifications to a specific patient.

3. Proof-of-Concept Assessment

The assessment of the process to generate a prosthetist-specific "global" template was divided into two steps. The first step evaluated whether the rectification rule learned by the AI was plausible and consistent with clinician expectations. The second step evaluated the feasibility of the template by applying the AI rectification process to a new participant and comparing the results of the AI rectification to the prosthetist's manual rectification of the same participant.

3.1. Assessment of the Rectification Rule Learned by the AI

Fourteen participants with transtibial amputation were included for this part of the study (Table 1), along with a prosthetist with over 25 years of experience fabricating custom sockets for this level of amputation. Casts from these participants were used to train the AI algorithm.

Table 1. Characteristics of the participants in the dataset (taken from the following clinical trial: NCT04141748). Participants 1–14 were used in the training dataset to create the AI algorithm that was then applied to Participant 15. ID: identifier; M: male; F: female; BMI: body mass index; R: right; L: left.

	Participant ID	Sex (M/F)	Age (years)	Mass (kg)	Height (cm)	BMI	Race	Ethnicity	Side (R/L)	Etiology	Residual Limb Length (cm)	Residual Limb Tissue Type
Training dataset	1	M	41	84	175	27.4	White	Hispanic or Latino	R	Congenital	12.5	Firm
	2	M	33	86	180	26.5	White	Hispanic or Latino	L	Trauma	15.3	Firm
	3	M	23	60	180	18.5	White	Hispanic or Latino	L	Trauma	21.0	Medium
	4	M	34	87	168	30.8	White	Hispanic or Latino	L	Trauma	17.0	Soft
	5	F	64	76	178	24.0	White	Hispanic or Latino	L	Trauma	15.0	Medium
	6	M	57	61	165	22.4	White	Hispanic or Latino	R	Trauma	23.5	Medium
	7	M	37	55	174	18.2	White	Hispanic or Latino	R	Trauma	11.5	Medium
	8	M	62	83	182	25.1	White	Hispanic or Latino	L	Trauma	15.0	Medium
	9	M	63	88	175	28.7	White	Hispanic or Latino	L	Trauma	12.5	Medium
	10	M	40	74	170	25.6	White	Hispanic or Latino	L	Trauma	23.2	Firm
	11	M	48	97	185	28.3	White	Hispanic or Latino	L	Congenital	12.5	Firm
	12	M	37	74	180	22.8	White	Hispanic or Latino	L	Trauma	18.2	Soft
	13	M	58	76	165	27.9	White	Hispanic or Latino	L	Trauma	16.0	Firm
	14	M	56	99	178	31.2	White	Hispanic or Latino	L	Trauma	20.0	Medium

Table 1. *Cont.*

Participant ID	Sex (M/F)	Age (years)	Mass (kg)	Height (cm)	BMI	Race	Ethnicity	Side (R/L)	Etiology	Residual Limb Length (cm)	Residual Limb Tissue Type
Average (1−14)	M (93%) F (7%)	47	79	175	25.5	White (100%)	Hispanic or Latino (100%)	L (79%) R (21%)	Trauma (86%) Congenital (14%)	16.7	Firm (36%) Medium (50%) Soft (14%)
15	M	62	94	187	26.9	White	Hispanic or Latino	L	Trauma	14.0	Firm

From the UPs of the participants obtained after step 9 (i.e., after morphing with the reference shape), we computed an average UP mesh using the PCA approach described in Steer et al. [35]. Then, the ADM was applied to this average UP to obtain an average Digital-RP mesh. A distance color map was built between the UP and the Digital-RP average meshes to qualitatively check whether the rectification rule learned by the AI was consistent with the prosthetist's written description of their rectification approach (see Figure 3). Moreover, to understand the synergistic changes the prosthetist applied to adapt each individual rectification from the typical rectification approach to a specific patient, the modes of variation learned by the AI were numbered and ranked based on the variance they explained. Then, the effect of each mode was visually inspected by the prosthetist, who varied the weighting factor of the mode from −3 to 3 (standard deviations), and by generating a new Digital-RP mesh, reflecting the combined effect of the ADM and the mode.

3.2. Application of the Prosthetist-Specific "Global" Template to a "New" Participant

To digitally rectify the UP of a new subject with the average AI-learned rule, the UP must be pre-processed and morphed with the Reference Mesh (steps 1–9 in previous section), and then the ADM applied, setting to zero the weighting factors for the modes of variation. To illustrate this process, the ADM obtained from 14 participants with transtibial amputation was applied to the UP morphed mesh of a 15th participant not included in the ADM calculation (Figure 5). The application of the ADM changes the position of each vertex of the mesh according to its respective mean displacement vector, obtaining a "Digital-RP" for participant 15.
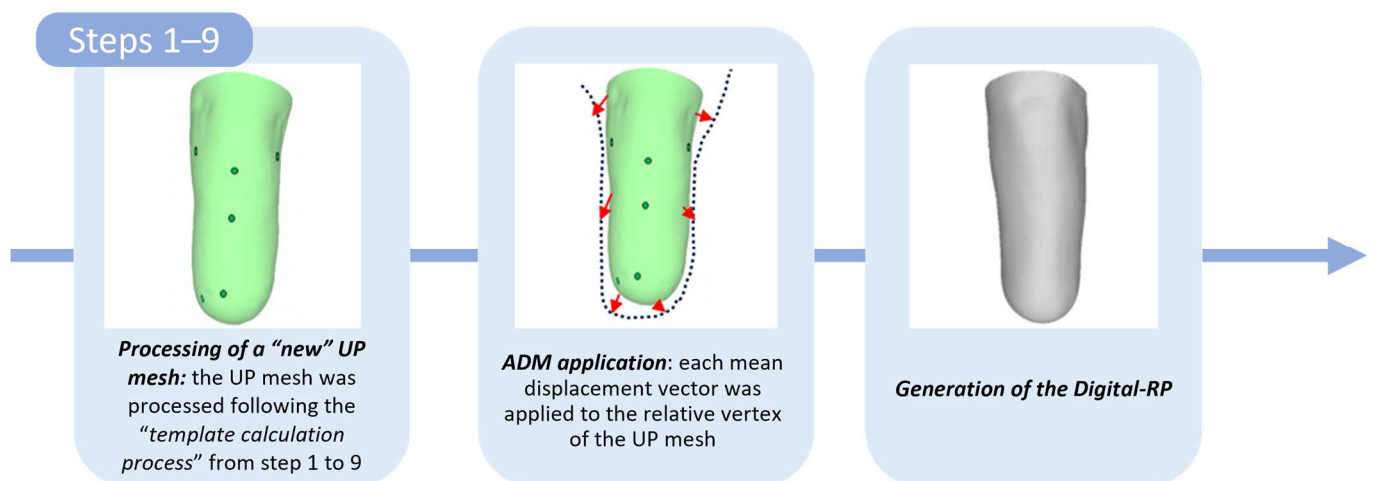

Steps 1–9

Processing of a "new" UP mesh: the UP mesh was processed following the "*template calculation process*" from step 1 to 9

ADM application: each mean displacement vector was applied to the relative vertex of the UP mesh

Generation of the Digital-RP

Figure 5. Schematic representation of the generation of the digital-rectified positive (Digital-RP) mesh of a "new" participant by applying the average displacement matrix (ADM), i.e., the global matrix, to the morphed-unrectified position (UP) mesh of the new participant. Dots in image indicate location of landmarks. The red arrows indicated the translation of the UP's vertices calculated by the ADM to generate the RP (represented by dotted line).

To assess the feasibility of the ADM prediction, the Digital-RP was compared to the scan of the participants' manual RP fabricated by the prosthetist (herein "Hand-RP") using three strategies based on the currently available, albeit limited, literature.

First, differences between the two meshes were qualitatively illustrated by means of color maps, representing the Radial Errors (REs) and Angle Errors (AEs), using previously described approaches [41,48–50]. The RE map depicts the distance between the meshes in the relative orientation of the surface of the meshes, i.e., shape changes. For instance, two meshes that are scaled one relative to the other, but which preserve parallel shapes, will show null differences in the AE map but differences in the RE map. On the contrary, almost overlapping meshes that present intersecting surfaces will show limited differences in the RE map and large differences in the AE map.

Second, we took advantage of the results provided by Dickinson et al. [49], who reported the repeatability of the RP handcrafted by a prosthetist when casting the same individual twice. We assumed that the Digital-RP in our study was plausible if it was within the limits of the within-prosthetist repeatability reported by Dickinson et al. [49], since the ADM prediction equated to a repeated cast by the same prosthetist on the same participant. Specifically, Dickinson et al. [49] described prosthetist repeatability using three outcome measures. The first measure was the absolute value of the RE (defined by Dickinson et al. [49] as the "absolute surface height"), reporting that it should be within 3.6 mm $\pm$ 1.96 $\times$ SD (SD = 0.81) when computed for 95% of the vertices of the mesh [49]. When considering only the vertices between the distal end and the MPT height, the absolute RE should be 2.87 mm $\pm$ 1.96 $\times$ SD (SD = 0.44) [49]. The second was the minimum detectable change (MDC) for cross-sectional perimeters (clinically referred to by prosthetists as circumferences) up to the MPT level, with a value of 3.53% [49]. The third measure was the MDC of the volume from the distal end to the MPT cross-section, with a value of 3.47% [49].

Finally, from the data reported by Fernie et al. [51] and Lilja et al. [52], we can state that, given a residual limb with a fixed volume and a well-fit socket, if this socket has a volume variation between −2.5% and 5%, the socket is still considered to fit well. Therefore, we assumed that the Digital-RP was plausible if the volume variation compared to the prosthetist Hand-RP was within this range.

4. Results

4.1. Assessment of the Rectification Rule Learned by the AI

Figure 6 illustrates the rectification technique learned by the AI. The typical rectifications performed by the prosthetist are described through a distance color map. This figure also shows the first four modes of variation identified by the AI algorithm in the order of explained variance. The variance profile is relatively flat, making it necessary to consider up to the ninth mode of variation to explain 90% of the total variance. These modes embed the specific rectifications created by the prosthetist to adapt the "average" rectifications to the individual characteristics of a new participant. For this particular prosthetist, the first mode was related to the distal end of the RP. The algorithm generated an average lengthening of the distal end of the digital model of 10 mm. This is consistent with the prosthetist's description of their rectification approach, which included the lengthening the distal end of the positive model by approximately 15 mm. The second mode was related to the creation of posterior flares to accommodate the flexor tendons when the knee flexes. For the remaining modes of variation, the rectifications appear related to the creation of reliefs (unloaded areas) for distal bony prominences or painful spots (e.g., neuromas). For example, the third mode was associated with a relief over the distal end of the fibula and the fourth mode was related to a relief over the anterior distal end of the tibia. Together, the first four modes explained 64% of the total variance.
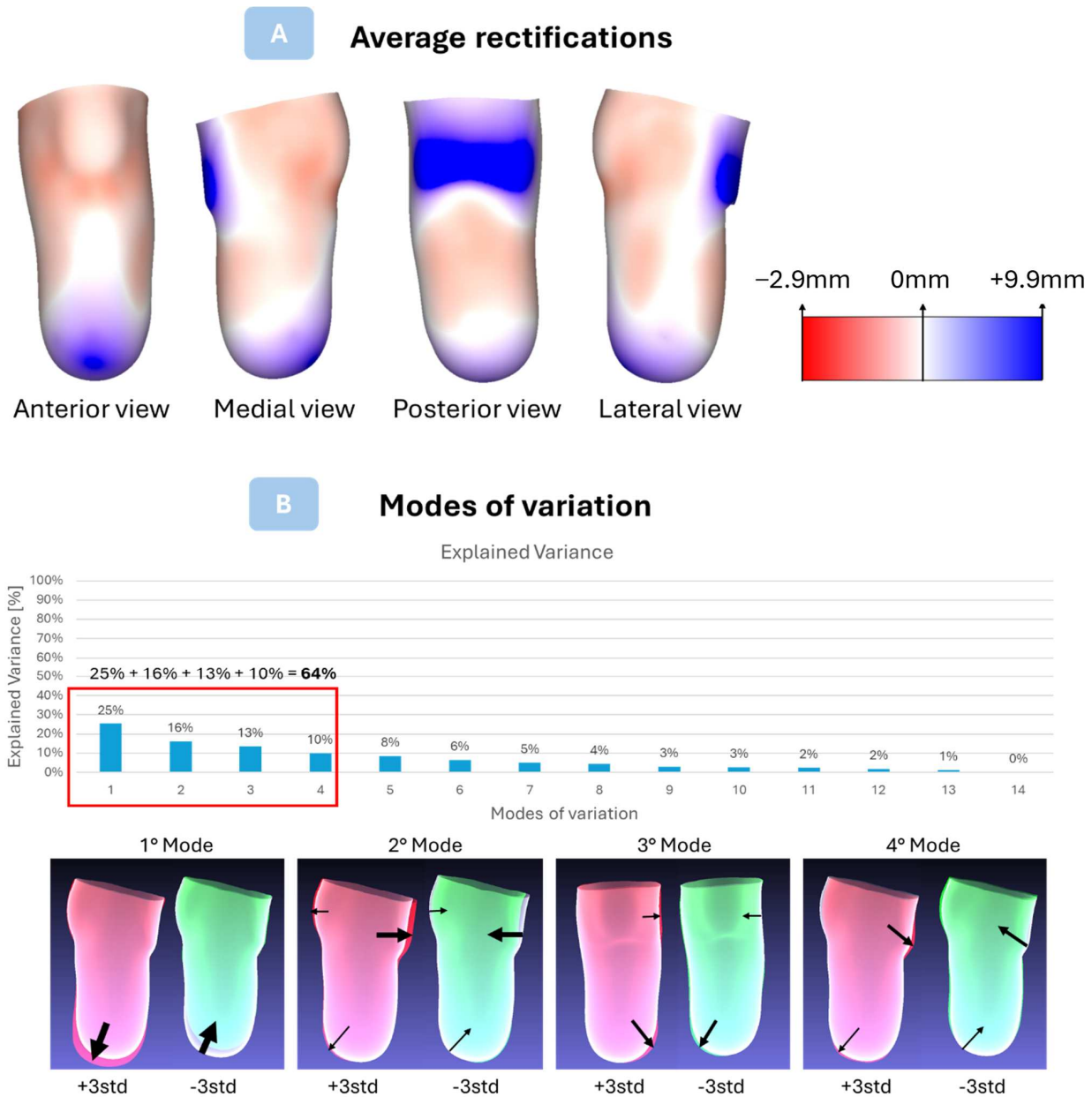
Figure 6. (**A**) Distance color maps in the Red–White–Blue scale describing the average rectifications created by the prosthetist during the rectification process. Red was associated with material decrease, blue was associated with material increase, and white was associated with no change. (**B**) Plot of the variance explained by each mode of variation and the corresponding qualitative description of the rectifications included in each of the first four modes of variation. Black arrows indicate location, direction and relative magnitude of rectifications made in each mode. std: standard deviation.

4.2. *Application of the Prosthetist-Specific "Global" Template to a "New" Participant*

In Figure 7, color maps representing the absolute RE between the "Hand-RP" (hand-crafted by the prosthetist) and the "Digital-RP" (obtained with the algorithm) are illustrated along with boxplots of the distribution of the absolute RE for both the full surface and the surface between the most distal end of the residual limb (A) and the MPT. Absolute RE comparisons between the Hand- and Digital-RPs demonstrated the variability that fell within the previously reported [49] within-prosthetist repeatability ranges for the rectification of the positive models. Statistical indices, specifically the Mean RE (MRE), Median RE (MedRE), and Interquartile Range of the RE (IQR RE), are reported in the tables incorporated in Figure 7.
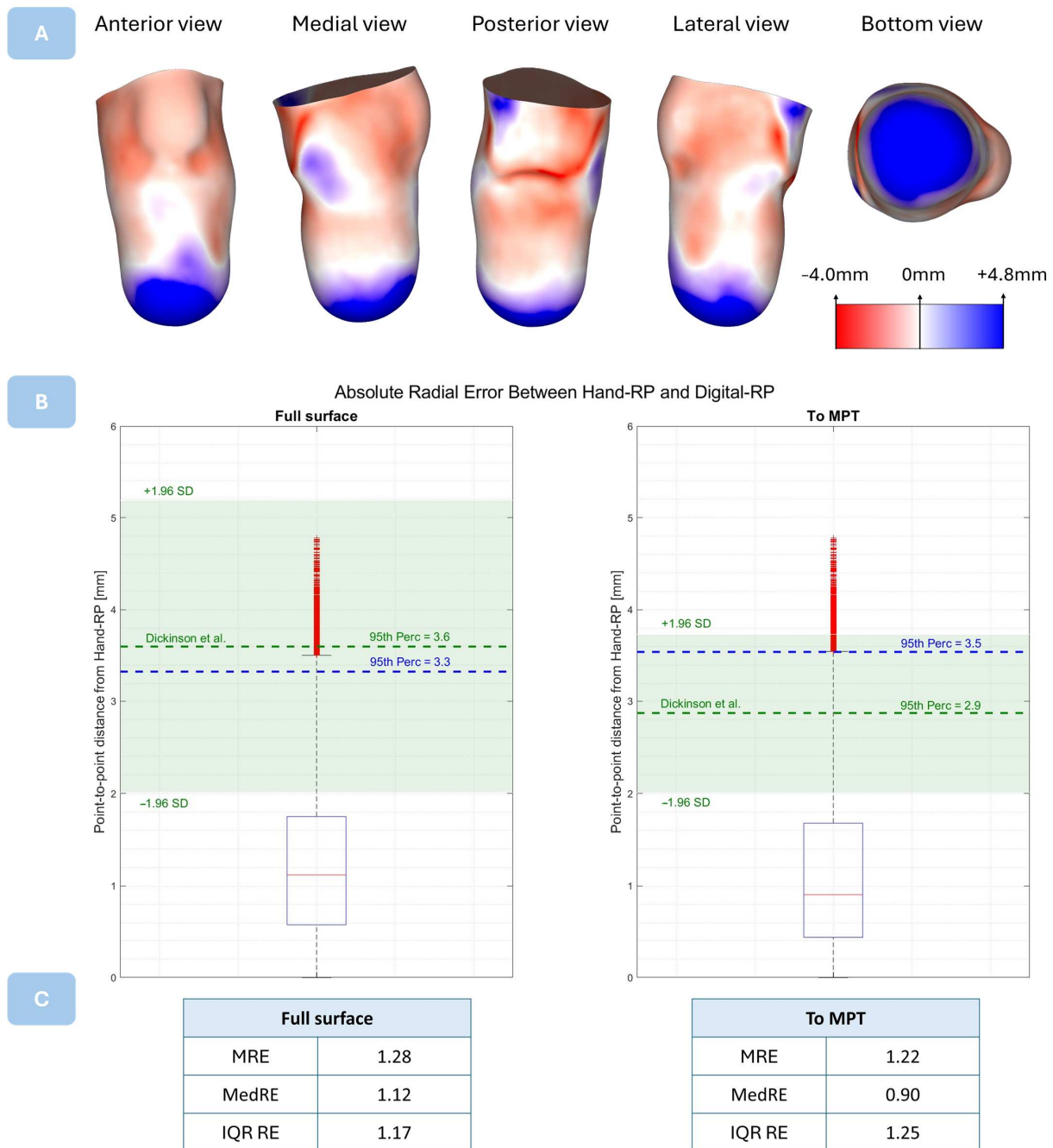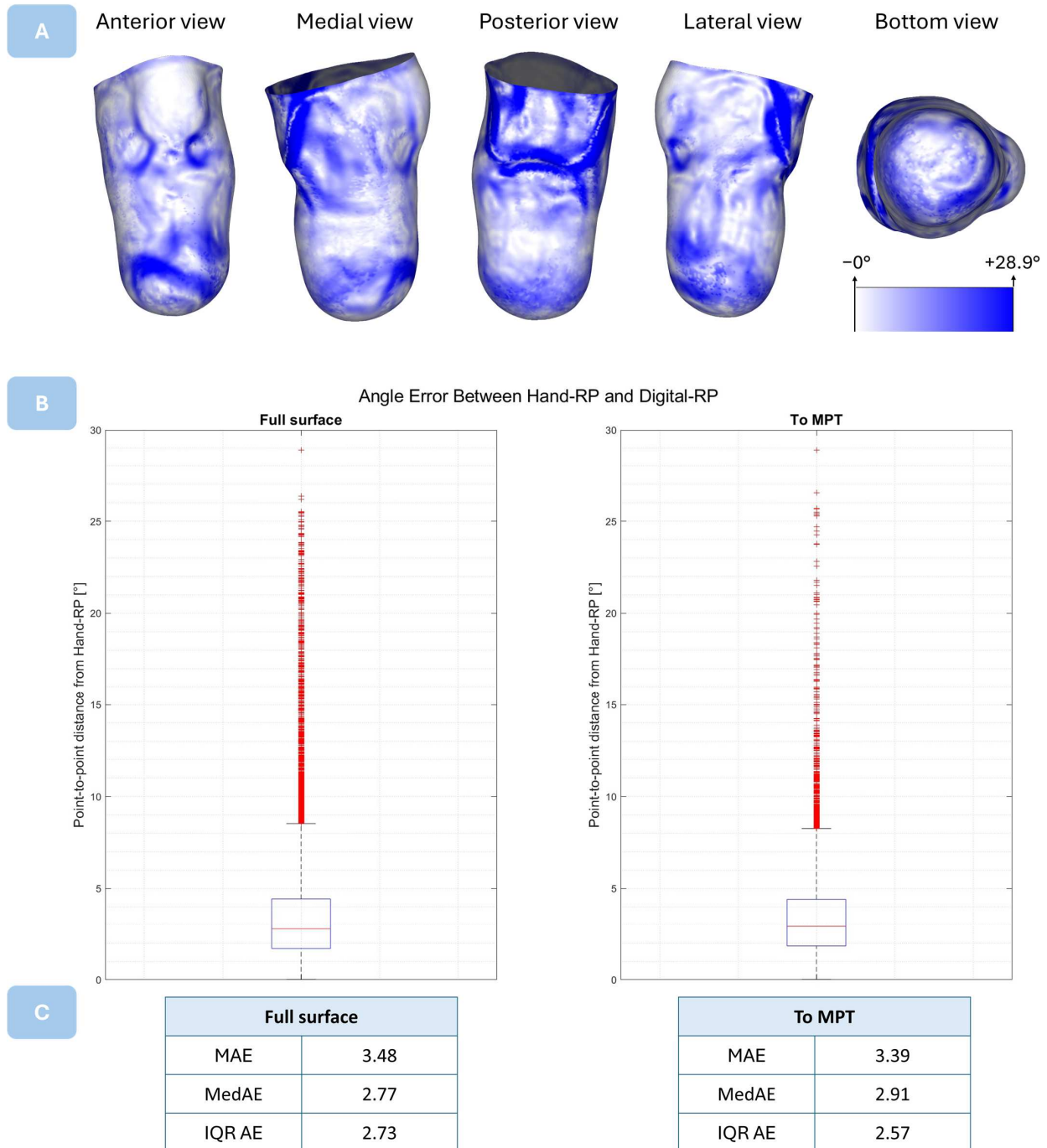
Figure 7. (**A**) Color maps of the absolute radial error (RE) comparing the hand-rectified positive (RP) and digital-rectified positive (RP) using the Red–White–Blue scale for the full surface (left) and for the surface between the most distal end of the residual limb (A) and the mid-patella tendon (MPT) (right). The most intense shade of red is associated with a material decrease of 4 mm, the most intense shade of blue is associated with a material increase of 4.8 mm, and white indicates no change. (**B**) Boxplots for the absolute RE for the full surface (left) and for the surface between A and the MPT (right). The blue dotted lines represent the 95th percentile of the absolute RE, while the green dotted line and green shaded area represent the mean and acceptable range from Dickinson et al. [49] of 2.01 to 5.19 mm for the full surface (left) and 2.01 to 3.73 mm between A and the MPT (right). (**C**) Statistical indices (Mean RE (MRE), Median RE (MedRE), and Interquartile Range (IQR) of the RE) for the full surface (left) and for the surface between A and the MPT (right).

In Figure 8, the differences between the Hand- and Digital-RPs are further highlighted by color maps of the AE, and boxplots illustrate the AE distributions for the full surface and

for the surface between the most distal end of the residual limb (A) and the MPT. Statistical indices, specifically the Mean AE (MAE), Median AE (MedAE), and Interquartile Range of the AE (IQR AE), are reported in the tables incorporated in Figure 8. Mean and Median AEs were smaller than 4°.

Full surface	
MAE	3.48
MedAE	2.77
IQR AE	2.73

To MPT	
MAE	3.39
MedAE	2.91
IQR AE	2.57

Figure 8. (**A**) Color maps of the Angle Error (AE) comparing the hand-rectified positive (RP) and digital-rectified positive (RP) using the Red–White–Blue scale, where the most intense shade of blue, associated with an AE of 28.9°, occurs in the flare of the posterior shelf, on the edge of the mid-patella tendon (MPT), and in a circular region distal to the end of the tibia. (**B**) Boxplots illustrating the AE between each corresponding vertex of the two meshes for the full surface (left) and for the surface between the most distal end of the residual limb (A) and the MPT (right). (**C**) Statistical indices (Mean AE (MAE), Median AE (MedAE), Interquartile Range (IQR) of the AE) for the full surface (left) and for the surface between A and the MPT (right).

In Figure 9, dimensional comparisons (radius and perimeters) between the Hand- and Digital-RPs for six equidistant cross-sections between the most distal end of the residual limb (A) and the MPT are illustrated. Percent differences in cross-sectional perimeters fell within the MDC reported by Dickinson et al. [49].
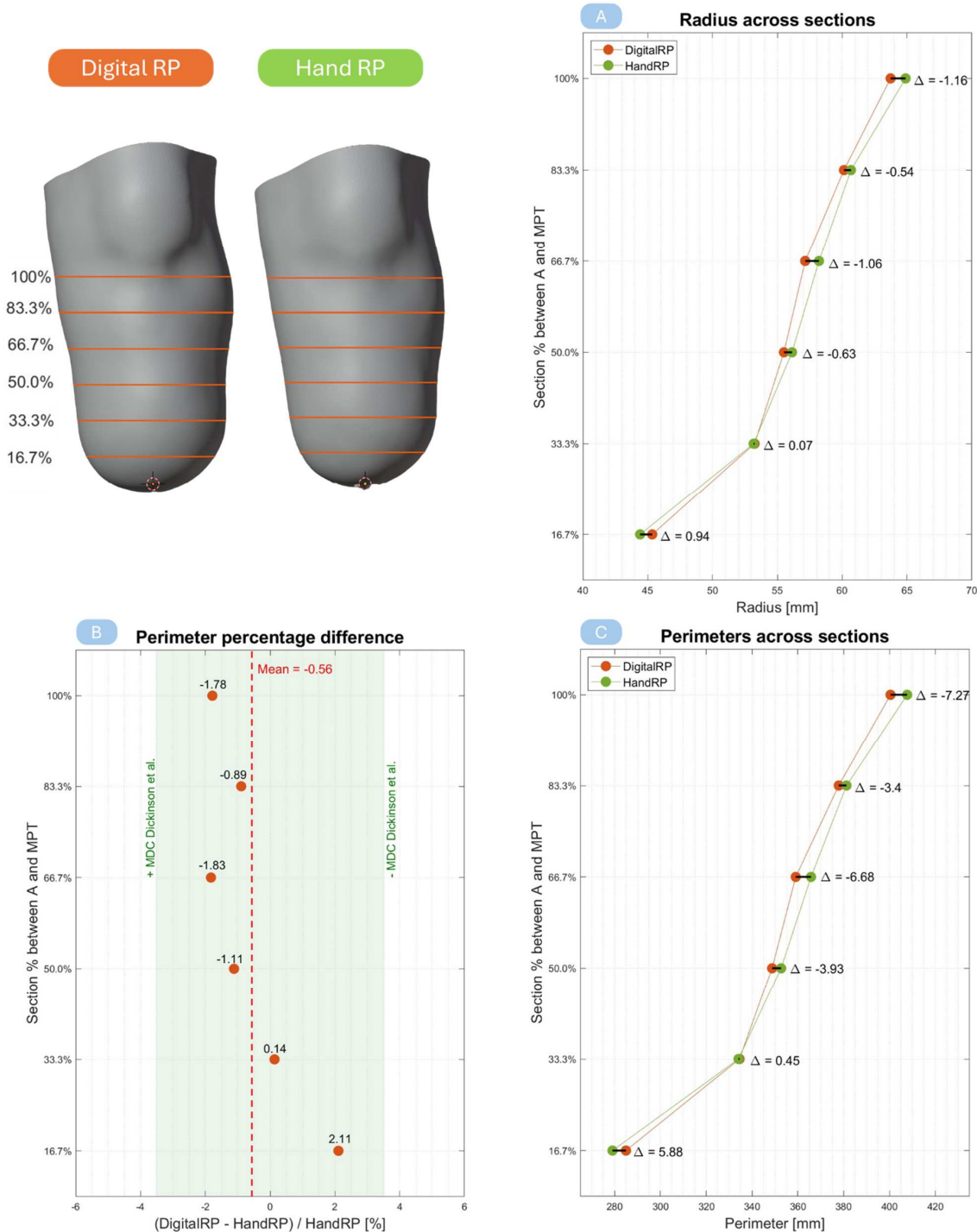
Figure 9. Dimensional comparisons between the hand-rectified positive (Hand-RP) and digital-rectified positive (Digital-RP) at 6 equidistant cross-sections between the most distal end of the residual limb (A) and the mid-patella tendon (MPT). (**A**) Difference in radii (in mm) at each cross-section. (**B**) Percentage difference in perimeters at each cross-section. Acceptable range shown in green shading using the Minimal Detectable Change (MDC) values reported by Dickinson et al. [49]. (**C**) Difference in perimeter (in mm) at each cross-section.

Finally, the percent volumetric difference for the volume enclosed between the most distal end of the residual limb (A) and the MPT between the meshes of the Hand- and Digital-RPs was calculated to be 0.65%. This volume difference was substantially less than the range of volume difference reported to affect the socket fit (−2.5% to 5%) [51,52].

5. Discussion

The aim of this work was to describe a novel process to generate a prosthetist-specific "global" template and to illustrate that it can be automatically applied to rectify the shape of the residual limb of a person with transtibial amputation. Our illustration suggests that the Digital-RP was (1) consistent with the description provided by the prosthetist of their approach to rectification, (2) had small differences in the RE and AE, and (3) had similar dimensions as the Hand-RP for the same participant, which were within the range of repeatability reported by Dickinson et al. [49].

Our proposal generates a global template in the form of a rule learned by an unsupervised AI algorithm, i.e., a set of PCA-derived matrices defining an average rectification, interpreted as the "typical" rectification approach of a single prosthetist, and a set of "modes of variation", i.e., the synergistic changes applied by the prosthetist when adapting their typical rectifications to a specific individual. The advantage of learning the synergistic changes is that the Digital-RP can account for the independent rectification of critical anatomical areas that occur in the Hand-RP, linking them and making explicit a missing piece of knowledge that, in our experience, prosthetists typically do not verbalize. This is a novel feature of our algorithm that may contribute to improving the education of novice prosthetists and patient care.

Once established, the global template can be applied to a new individual using the following two basic approaches: simply apply the average rectification (fully automated approach) or the prosthetist decides which modes of variation to apply and to what scale by knowing that their maximum weight is limited from −3 to 3 (standard deviations), where more extreme values correspond to more unusual changes (the semi-automated approach). Ultimately, the global template is an AI-assisted manufacturing tool and the final rectification produced by the algorithm (even when using the fully automated approach) must be approved by a prosthetist. It is possible that, for prosthetists, receiving feedback regarding their approach as learned by the AI algorithm may lead to a deeper understanding and better verbalization of their own approach to rectification. In our vision of clinical implementation, the global template would support the prosthetist in limiting time spent on the fabrication of the socket in favor of the time spent with patients, thereby understanding their clinical presentation and functional goals and troubleshooting prosthesis issues. In resource-limited settings and isolated communities, the availability of global templates based on experienced prosthetists who are recognized for their expertise in creating well-fitting sockets can support novice clinical professionals to improve patient outcomes. Finally, a Digital-RP can be easily used in the process of creating a customized socket using CAM solutions (e.g., 3D-printed sockets).

Before any global template can be implemented in clinical practice, it is important to establish its clinical validity. Our evaluation of clinical validity was limited to a proof-of-concept using a dataset of individuals with transtibial amputation. While we believe that our approach has merit and could also be relatively easily applied to individuals with transfemoral amputation, further studies are needed to support clinical application. Unfortunately, our ability to validate the AI algorithm was limited by the paucity of literature defining quantitative metrics for the rectification process. Using the available evidence, we identified a novel set of outcomes that we hope will be useful in further development.

We are aware of only a single study [49] reporting the within-prosthetist rectification repeatability in terms of the absolute RE and MDC for cross-sectional perimeters and residual limb volumes. Our results for the absolute RE comparisons between Hand- and Digital-RPs suggest that the variability introduced by the AI algorithm falls within the reported range of within-prosthetist repeatability [49] (Figure 7B). Similarly, our results

for the percent difference in cross-sectional perimeters are within the MDC range [49] (Figure 9B). While it is positive that our results did not exceed the ranges reported by Dickinson et al. [49], it may not be an entirely fair comparison. It should be noted that Dickinson et al. [49] assessed patella tendon-bearing sockets, while, in our study, the prosthetist's rectifications were intended to create a total surface-bearing socket which, by design, requires rectifications of a smaller magnitude.

When considering the color maps for the RE and AE, most differences occurred at the distal end of the residual limb and the proximal posterior flares, which are consistent with the regions reported by Dickinson et al. [49] to have the greatest "surface height" deviation between casts within-prosthetist. In practical terms, mismatches in these regions will not result in a critical failure of the socket fit, as they may be easily addressed on a thermoformable diagnostic socket during the fitting process by heating and modifying these socket regions by hand or adding a distal pad.

Similarly, a limited number of studies [51–55] have been published reporting the acceptability of sockets using changes in volume. These studies indicate that a −2.5% to 5% change in residual limb volume does not disrupt the socket fit. Our results for the volume encompassed between the distal end of the residual limb and the MPT were within the "good fit" range of −2.5% to 5% [51,52]. Overall, we believe that the AI predictions are plausible, within the limits of the prosthetist's own repeatability, and within the limits of an acceptable socket fit if the hand cast itself resulted in an acceptable fit.

It should be noted that we asked all of the prosthetists involved in the larger clinical study [39] to use the rectification method they were most confident with, and all of them preferred to manually modify the plaster positive molds. This leads us to question whether the rectification software currently available is sufficient in meeting the needs of all prosthetists. If this is the case, a new category of software may help prosthetists in the digital production of sockets.

The limitations of the proposed process used to generate the algorithm include the use of 15 physical LMs. Their identification and application within the physical mold can be time-consuming. Future research should explore the minimum marker set required to achieve the suitable spatial registration of the meshes and the morphing of the reference mesh. The proposed process is also reliant on the availability of a good quality structured light 3D scanner and digital processing procedures. Datasets with poor quality will result in the poor training of the AI algorithm. This initial proof-of-concept was limited to the training of the AI on a dataset of 14 subjects that did not consider the socket comfort ultimately experienced by the participants when using sockets made from the Hand-RP. To better assess the potential of the AI algorithm to generate well-fitting initial sockets, it will be necessary to use training datasets with more participants that include data only from sockets deemed comfortable by participants for everyday use. It is possible that, to achieve this, additional participant characteristics may need to be included as part of training the AI algorithm, e.g., participant age, soft-tissue consistency, the expected activity level, etc.

6. Conclusions

This study provides a proof-of-concept of the integration of an AI algorithm in the fabrication process of transtibial prosthetic sockets. We illustrated that the algorithm can learn the typical rectifications performed by a prosthetist during the manual rectification of a UP mold to obtain the respective RP mold. Fundamental to the success of the process was the implementation of a novel step-by-step dataset acquisition and processing procedure coupled with a "morphing" phase that ensured the UP-RP pairs had the same topology. Once refined, this approach may provide a useful time-saving tool for prosthetists, automatically implementing typical rectifications, and provide a good starting socket fit for individuals with amputation. Finally, the creation of templates based on the rectification techniques of highly skilled prosthetists could provide a valuable tool in areas lacking sufficient prosthetists.

Abbreviations

3D	three dimensional
A	distal end of the residual limb
ADM	average displacement matrix
AF	distal fibula
AEs	angle errors
AI	artificial intelligence
CAD	computer-aided design
CAD-CAM	computer-aided design–computer-aided manufacturing
Digital-RP	digital-rectified positive
FAT	anterior distal tibia
Hand-RP	hand-rectified positive
HF	head of the fibula
ICP	iterative closest point algorithm
ID	identifier
IQR	interquartile range
LC	lateral condyle

LM	landmark
MAE	mean angle error
MAT	medial distal tibia
MedAE	median angle error
MC	medial condyle
MCT	medial condyle of the tibia
MDC	minimal detectable change
MPT	mid-patella tendon
MRE	mean radial error
MedRE	median radial error
PAD	one-third of the P-A distance—distal
PAP	one-third of the P-A distance—proximal
PCA	principal component analysis
PF	popliteal fossa
RCMs	rectification color maps
REs	radial errors
RP	rectified positive
SD	standard deviation
SVD	singular value decomposition
SS	below semitendinosus/semimembranosus at knee flexion of 90°
TT	tibial tuberosity
UP	unrectified positive

Appendix A

This appendix provides further details regarding the mesh procedures described in the "Materials and Methods" section of the manuscript.

Mesh Alignment Procedure in Global Coordinate System

The alignment procedure used in the manuscript is based on the location of four landmarks, which are necessary to identify the axes and planes. The important landmarks for this purpose are the mid-patellar tendon (MPT), the popliteal fossa (PF), the most distal end of the residual limb (A), and the anterior distal end of the tibia (FAT). The alignment of each unrectified positive scan was performed as follows:

1. Identify the anatomic z-axis (z_{anat}) passing through A and the midpoint between the MPT and PF;
2. Cut the mesh with a plane passing through the MPT, perpendicular to z_{anat}, since only the distal part of the UP is necessary to perform the alignment;
3. Identify a temporary y-axis (y_{temp}) by tracing the normal to the plane passing through the FAT, MPT, PF, and A;
4. Define the x-axis so as to be perpendicular to both the z-axis and y-temp, as follows:

$$x = \frac{y_{temp} \times z_{anat}}{||z_{anat} \cdot x||}$$

5. Finally, determine the definitive y-axis so as to be perpendicular to z and x-axis, as follows:

$$y = \frac{z_{anat} \times x}{||z_{anat} \cdot x||}$$

As an additional step, automatic alignment results can be adjusted by the prosthetist based on their knowledge of the patient-specific anatomical condition and body posture.

Reference Mesh Generation

The Reference Mesh is characterized by a homogeneous topology and by a morphology that is representative of an average transtibial residual limb shape. To build this mesh, the unrectified positives (UPs) were pre-processed as described in Figure 3 (of the manuscript) up to step 8. Then, one of the UPs from the dataset was used as a "Temporary Reference"

to morph the other UPs. For this purpose, the 13th participant of the dataset was used, because their residual limb shape was considered by the investigators to be intermediate with respect to the others in the dataset (Figure A1). Then, morphed UPs, characterized by the same topology as the Temporary Reference, were used to obtain the mean shape of the dataset, evaluating the position of each vertex as the average position of the homologous vertices in each morphed UP. The average shape was then smoothed and re-meshed to obtain a more homogeneously distributed topology (Figure A2). Finally, landmarks (LMs) were projected from the mesh before to the mesh after re-meshing to associate each LM to its new vertex identifier (ID).
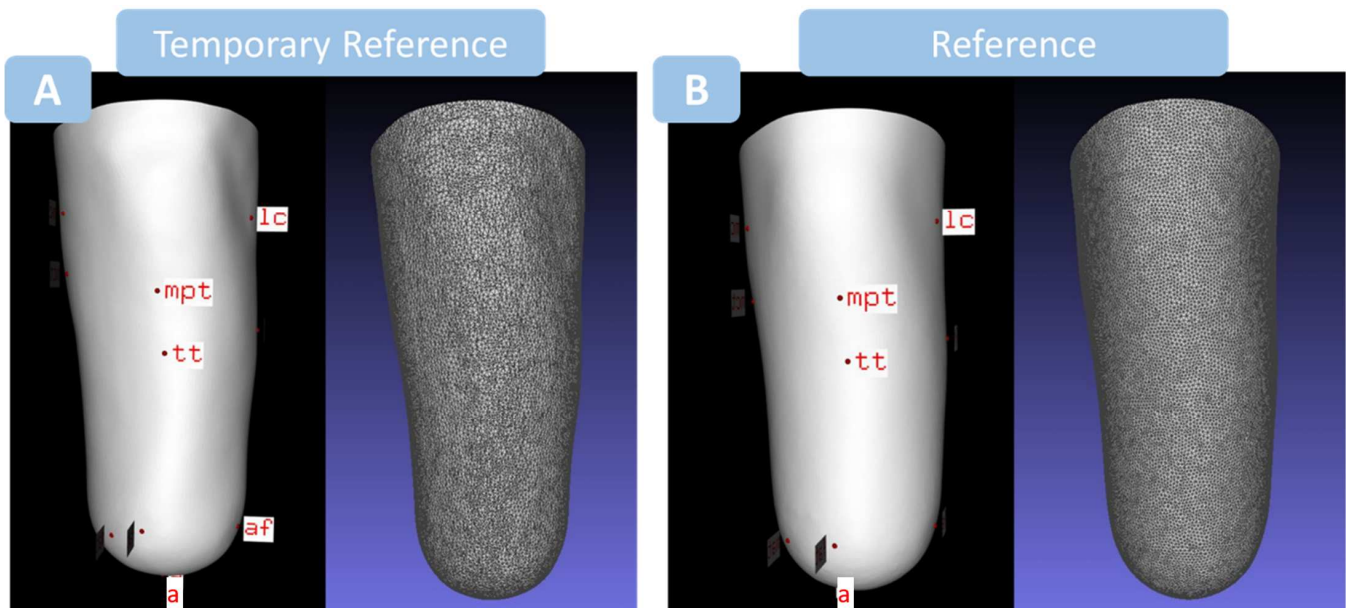

Figure A1. (**A**) Landmark labeling and mesh representation of the Temporary Reference used during morphing to obtain the final Reference Mesh; (**B**) Landmark labeling and mesh representation of the Reference Mesh used to perform morphing during the pre-processing of meshes used to build a rectification color map. LC: lateral condyle; MPT: mid-patellar tendon; TT: transtibial; AF: distal end of the fibula; A: most distal end of the residual limb.

Morphing Procedure

The morphing procedure is a fundamental step in mesh pre-processing for the application of the AI algorithm described in the manuscript. This operation aims to obtain meshes with a homogeneous topology, specifically the same vertices and faces of a Reference Mesh. The morphing procedure was implemented through the Radial Basis Function (RBF) method [47] (RBF-Morph, Rome, Italy).

In this study, the procedure to morph the Reference Mesh onto a target mesh was divided into the following two phases (Figure A2):

- First phase: the LMs and vertices of the Reference Mesh were overlapped to the respective homologous vertices of the target mesh, leading to a first approach between these two meshes.
- Second phase: an iterative closest point (ICP) optimization process was used to fit the topology of the reference mesh onto the shape of the target using RBF.
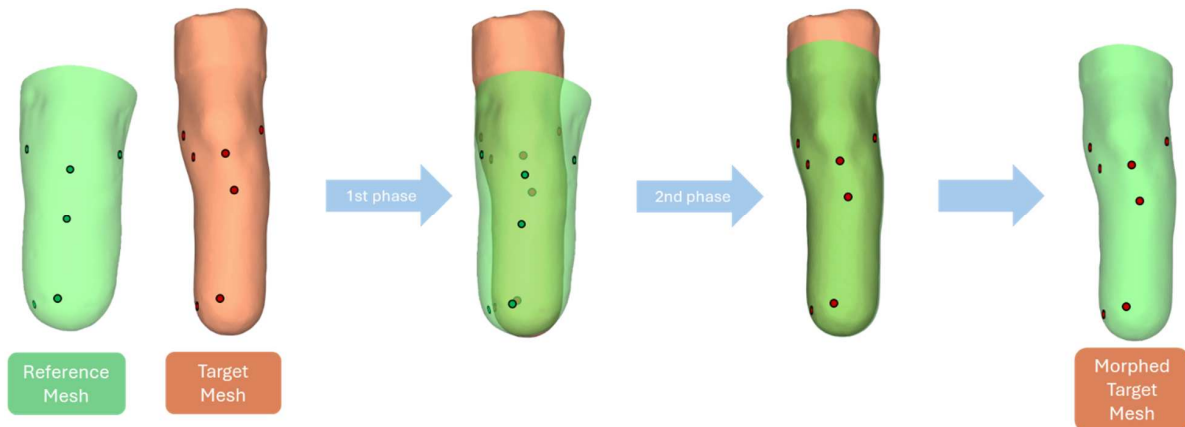
Figure A2. Illustration of the morphing process. Dots in image indicate location of landmarks.

The output of this two-step procedure was a mesh characterized by the same topology (vertices and faces) as the Reference Mesh, but with the shape of the "target" mesh.

For the purposes of this study, pairs of unrectified (UP) and rectified (RP) positives of the same participant were morphed to later assess the displacement vectors between homologous vertices. To effectively map the differences/displacements between these coupled meshes, first the Reference Mesh was morphed onto the UP mesh, and then the UP mesh was in turn morphed onto the respective RP mesh (Figure A3). This way, homologous vertices were mapped as far as possible in correspondence with the anatomical areas between the UP and RP meshes.
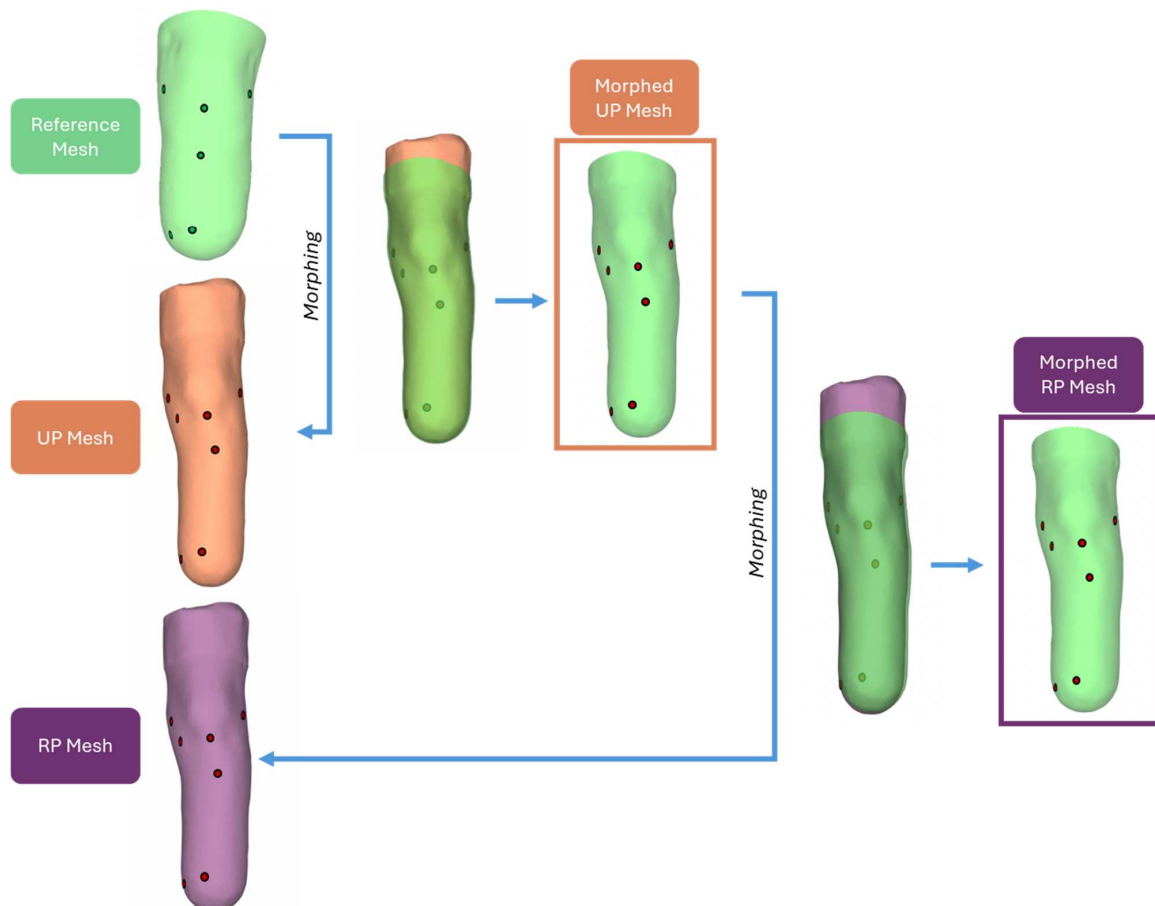

Figure A3. Graphical representation of the morphing procedure implemented in this study to morph pairs of unrectified positive–rectified positive (UP-RP) meshes. Dots in image indicate location of landmarks.

References

1. Cutti, A.G.; Morosato, F.; Gentile, C.; Gariboldi, F.; Hamoui, G.; Santi, M.G.; Teti, G.; Gruppioni, E. A workflow for studying the stump-socket interface in persons with transtibial amputation through 3D thermographic mapping. *Sensors* **2023**, *23*, 5035. [CrossRef] [PubMed]

2. Paterno, L.; Ibrahimi, M.; Gruppioni, E.; Menciassi, A.; Ricotti, L. Sockets for limb prostheses: A review of existing technologies and open challenges. *IEEE Trans. Biomed. Eng.* **2018**, *65*, 1996–2010. [CrossRef] [PubMed]

3. Mak, A.F.; Zhang, M.; Boone, D.A. State-of-the-art research in lower-limb prosthetic biomechanics-socket interface: A review. *J. Rehabil. Res. Dev.* **2001**, *38*, 161–174. [PubMed]

4. Safari, M.R.; Rowe, P.; McFadyen, A.; Buis, A. Hands-off and hands-on casting consistency of amputee below knee sockets using magnetic resonance imaging. *Sci. World J.* **2013**, *2013*, 486146. [CrossRef] [PubMed]

5. Cullen, S.; Mackay, R.; Mohagheghi, A.; Du, X. The use of smartphone photogrammetry to digitise transtibial sockets: Optimisation of method and quantitative evaluation of suitability. *Sensors* **2021**, *21*, 8405. [CrossRef]

6. Olsen, J.; Turner, S.; Chadwell, A.; Dickinson, A.; Ostler, C.; Armitage, L.; McGregor, A.; Dupan, S.; Day, S. The impact of limited prosthetic socket documentation: A researcher perspective. *Front. Rehabil. Sci.* **2022**, *3*, 853414. [CrossRef]

7. Fatone, S.; Johnson, W.B.; Tran, L.; Tucker, K.; Mowrer, C.; Caldwell, R. Quantification of rectifications for the Northwestern University Flexible Sub-Ischial Vacuum Socket. *Prosthet. Orthot. Int.* **2017**, *41*, 251–257. [CrossRef]

8. Boone, D.A.; Burgess, E.M. Automated Fabrication of Mobility Aids: Clinical demonstration of the UCL computer aided socket design system. *J. Prosthet. Orthot.* **1989**, *1*, 187–190. [CrossRef]

9. Mayo, A.L.; Gould, S.; Cimino, S.R.; Glasford, S.; Harvey, E.; Ratto, M.; Hitzig, S.L. A qualitative study on stakeholder perceptions of digital prosthetic socket fabrication for transtibial amputations. *Prosthet. Orthot. Int.* **2022**, *46*, 607–613. [CrossRef]

10. Fatone, S.; Caldwell, R. Northwestern University Flexible Subischial Vacuum Socket for persons with transfemoral amputation: Part 2 Description and preliminary evaluation. *Prosthet. Orthot. Int.* **2017**, *41*, 246–250. [CrossRef]

11. Rubin, G.; Fischer, E.; Dixon, M. Prescription of above-knee and below-knee prostheses. *Prosthet. Orthot. Int.* **1986**, *10*, 117–124. [CrossRef] [PubMed]

12. Long, I. Technical Note: Allowing normal adduction of femur in above-knee amputations. *Orthot. Prosthet.* **1975**, *29*, 53–54.

13. Alley, R.; Williams, T.; Albuquerque, M.; Altobelli, D. Prosthetic sockets stabilized by alternating areas of compression and release. *J. Rehabil. Res. Dev.* **2011**, *48*, 679–696. [CrossRef] [PubMed]

14. Moo, E.K.; Abu Osman, N.A.; Pingguan-Murphy, B.; Wan Abas, W.A.B.; Spence, W.D.; Solomonidis, S.E. Interface pressure profile analysis for patellar tendon-bearing socket and hydrostatic socket. *Acta Bioeng. Biomech.* **2009**, *11*, 37–43.

15. Söderberg, B. A new trim line concept for trans-tibial amputation prosthetic sockets. *Prosthet. Orthot. Int.* **2002**, *26*, 159–162. [CrossRef]

16. Stevens, P.M.; DePalma, R.R.; Wurdeman, S.R. Transtibial socket design, interface, and suspension: A clinical practice guideline. *J. Prosthet. Orthot.* **2019**, *31*, 172–178. [CrossRef]

17. Raschke, S.U. Limb Prostheses: Industry 1.0 to 4.0: Perspectives on technological advances in prosthetic care. *Front. Rehabil. Sci.* **2022**, *3*, 854404. [CrossRef]

18. Steer, J.; Stocks, O.; Parsons, J.; Worsley, P.; Dickinson, A. Ampscan: A lightweight Python package for shape analysis of prosthetics and orthotics. *J. Open Source Softw.* **2020**, *5*, 2060. [CrossRef]

19. Karakoç, M.; Batmaz, İ.; Sariyildiz, M.A.; Yazmalar, L.; Aydin, A.; Em, S. Sockets manufactured by CAD/CAM method have positive effects on the quality of life of patients with transtibial amputation. *Am. J. Phys. Med. Rehabil.* **2017**, *96*, 578–581. [CrossRef]

20. Tay, F.E.H.; Manna, M.A.; Liu, L.X. A CASD/CASM method for prosthetic socket fabrication using the FDM technology. *Rapid Prototyp. J.* **2002**, *8*, 258–262. [CrossRef]

21. Travis, R.P.; Dewar, M.E. Computer-aided socket design for trans-femoral amputees. *Prosthet. Orthot. Int.* **1993**, *17*, 172–179. [CrossRef] [PubMed]

22. Houston, V.L.; Burgess, E.M.; Childress, D.S.; Lehneis, H.R.; Mason, C.P.; Garbarini, M.A.; LaBlanc, K.P.; Boone, D.; Chan, R.B.; Harlan, J.H.; et al. Automated fabrication of mobility aids (AFMA): Below-knee CASD/CAM testing and evaluation program results. *J. Rehabil. Res. Dev.* **1992**, *29*, 78–124. [CrossRef] [PubMed]

23. Engsberg, J.R.; Clynch, G.S.; Lee, A.G.; Allan, J.S.; Harder, J.A. A CAD CAM method for custom below-knee sockets. *Prosthet. Orthot. Int.* **1992**, *16*, 183–188. [CrossRef] [PubMed]

24. Torres-Moreno, R.; Saunders, C.G.; Foort, J.; Morrison, J.B. Computer-aided design and manufacture of an above-knee amputee socket. *J. Biomed. Eng.* **1991**, *13*, 3–9. [CrossRef] [PubMed]

25. Köhler, P.; Lindh, L.; Netz, P. Comparison of CAD-CAM and hand made sockets for PTB prostheses. *Prosthet. Orthot. Int.* **1989**, *13*, 19–24. [CrossRef]

26. Krouskop, T.A.; Muilenberg, A.L.; Doughtery, D.R.; Winningham, D.J. Computer-aided design of a prosthetic socket for an above-knee amputee. *J. Rehabil. Res. Dev.* **1987**, *24*, 31–38.

27. van der Stelt, M.; Grobusch, M.P.; Koroma, A.R.; Papenburg, M.; Kebbie, I.; Slump, C.H.; Maal, T.J.J.; Brouwers, L. Pioneering low-cost 3D-printed transtibial prosthetics to serve a rural population in Sierra Leone—An observational cohort study. *eClinicalMedicine* **2021**, *35*, 100874. [CrossRef]

28. Tsai, T.F.; Maibach, H.I. How irritant is water? An overview. *Contact Dermat.* **1999**, *41*, 311–314. [CrossRef]

29. Kim, S.; Chen, J.; Cheng, T.; Gindulyte, A.; He, J.; He, S.; Li, Q.; Shoemaker, B.A.; Thiessen, P.A.; Yu, B.; et al. PubChem 2023 update. *Nucleic Acids Res.* **2023**, *6*, D1373–D1380. [CrossRef]

30. Anderson, S.; Stuckey, R.; Oakman, J. Work-related musculoskeletal injuries in prosthetists and orthotists in Australia. *Int. J. Occup. Saf. Ergon.* **2021**, *27*, 708–713. [CrossRef]

31. Sidles, J.A.; Boone, D.; Harlan, J.S.; Burgess, E.M. Rectification maps: A new method for describing residual limb and socket shapes. *J. Prosthet. Orthot.* **1989**, *1*, 149–153. [CrossRef]

32. Lemaire, E.D.; Johnson, F. A quantitative method for comparing and evaluating manual prosthetic socket modifications. *IEEE Trans. Rehabil. Eng.* **1996**, *4*, 303–309. [CrossRef] [PubMed]

33. Lemaire, E.D.; Bexiga, P.; Johnson, F.; Solomonidis, S.E.; Paul, J.P. Validation of a quantitative method for defining CAD/CAM socket modifications. *Prosthet. Orthot. Int.* **1999**, *23*, 30–44. [CrossRef]

34. Dickinson, A.S.; Diment, L.; Morris, R.; Pearson, E.; Hannett, D.; Steer, J. Characterising residual limb morphology and prosthetic socket design based on expert clinician practice. *Prosthesis* **2021**, *3*, 280–299. [CrossRef]

35. Steer, J.W.; Worsley, P.R.; Browne, M.; Dickinson, A.S. Predictive prosthetic socket design: Part 1-population-based evaluation of transtibial prosthetic sockets by FEA-driven surrogate modelling. *Biomech. Model. Mechanobiol.* **2020**, *19*, 1331–1346. [CrossRef] [PubMed]

36. Steer, J.W.; Grudniewski, P.A.; Browne, M.; Worsley, P.R.; Sobey, A.J.; Dickinson, A.S. Predictive prosthetic socket design: Part 2-generating person-specific candidate designs using multi-objective genetic algorithms. *Biomech. Model. Mechanobiol.* **2020**, *19*, 1347–1360. [CrossRef]

37. Fernie, G.R.; Halsall, A.P.; Ruder, K. Shape sensing as an educational aid for student prosthetists. *Prosthet. Orthot. Int.* **1984**, *8*, 87–90. [CrossRef]

38. Klasson, B. Computer aided design, computer aided manufacture and other computer aids in prosthetics and orthotics. *Prosthet. Orthot. Int.* **1985**, *9*, 3–11. [CrossRef]

39. Gard, S. Comparative Effectiveness of Socket Casting Methods: Improving Form and Fit. Available online: https://clinicaltrials.gov/study/NCT04141748 (accessed on 16 September 2024).

40. Verein Deutscher Ingenieure, e.V. *VDI/VDE 2634, Optical 3D Measurement Systems—Multiple View Systems Based on Area Scanning*; Engl. VDI/VDE-Gesellschaft Mess- und Automatisierungstechnik: Dusseldorf, Germany, 2008; Available online: https://www.vdi.de/en/home/vdi-standards/details/vdivde-2634-blatt-3-optical-3d-measuring-systems-multiple-view-systems-based-on-area-scanning (accessed on 26 March 2024).

41. Cutti, A.G.; Santi, M.G.; Hansen, A.H.; Fatone, S. Accuracy, repeatability, and reproducibility of a hand-held structured-light 3D scanner across multi-site settings in lower limb prosthetics. *Sensors* **2024**, *24*, 2350. [CrossRef]

42. Cignoni, P.; Callieri, M.; Corsini, M.; Dellepiane, M.; Ganovelli, F.; Ranzuglia, G. MeshLab: An open-source Mesh processing tool. *Computing* **2008**, *1*, 129–136.

43. Schroeder, W.; Martin, K.; Lorensen, B.; Kitware Inc. *The Visualization Toolkit: An Object-Oriented Approach to 3D Graphics*; Kitware: New York, NY, USA, 2006.

44. Qt Company Ltd. Qt for Python. Available online: https://doc.qt.io/qtforpython-6/index.html#documentation (accessed on 21 June 2023).

45. Bunton, S.L.; Kutz, J.N. *Data-Driven Science and Engineering: Machine Learning, Dynamical Systems, and Control*; Cambridge University Press: Cambridge, UK, 2019.

46. Zhang, Z. Iterative point matching for registration of free-form curves and surfaces. *Int. J. Comp. Vis.* **1994**, *13*, 119–152. [CrossRef]

47. Biancolini, M.E. *Fast Radial Basis Functions for Engineering Applications*; Springer: Cham, Switzerland, 2018. [CrossRef]

48. Sanders, J.E.; Severance, M.R.; Allyn, K.J. Computer-socket manufacturing error: How much before it is clinically apparent? *J. Rehabil. Res. Dev.* **2012**, *49*, 567–582. [CrossRef] [PubMed]

49. Dickinson, A.S.; Donovan-Hall, M.K.; Kheng, S.; Bou, K.; Tech, A.; Steer, J.W.; Metcalf, C.D.; Worsley, P.R. Selecting appropriate 3D scanning technologies for prosthetic socket design and transtibial residual limb shape characterization. *J. Prosthet. Orthot.* **2022**, *34*, 33–43. [CrossRef]

50. Seminati, E.; Talamas, D.C.; Young, M.; Twiste, M.; Dhokia, V.; Bilzon, J.L.J. Validity and reliability of a novel 3D scanner for assessment of the shape and volume of amputees' residual limb models. *PLoS ONE* **2017**, *12*, e0184498. [CrossRef] [PubMed]

51. Fernie, G.R.; Holliday, P.J. Volume fluctuations in the residual limbs of lower limb amputees. *Arch. Phys. Med. Rehabil.* **1982**, *63*, 162–165. [PubMed]

52. Lilja, M.; Oberg, T. Volumetric determinations with CAD/CAM in prosthetics and orthotics: Errors of measurement. *J. Rehabil. Res. Dev.* **1995**, *32*, 141–148.

53. Sanders, J.E.; Fatone, S. Residual limb volume change: Systematic review of measurement and management. *J. Rehabil. Res. Dev.* **2011**, *48*, 949–986. [CrossRef]

54. Sanders, J.E.; Youngblood, R.T.; Hafner, B.J.; Cagle, J.C.; McLean, J.B.; Redd, C.B.; Dietrich, C.R.; Ciol, M.A.; Allyn, K.J. Effects of socket size on metrics of socket fit in trans-tibial prosthesis users. *Med. Eng. Phys.* **2017**, *44*, 32–43. [CrossRef]

55. van Stuivenberg, C.; de Laat, F.; Meijer, R.; van Kuijk, A. Inter- and intra-observer reproducibility and validity of an indirect volume measurement in transtibial amputees. *Prosthet. Orthot. Int.* **2010**, *34*, 20–30. [CrossRef]